

Prediction Using a Bayesian Heteroscedastic Composite Gaussian Process

Casey B. Davis^a, Christopher M. Hans^b, Thomas J. Santner^c

Department of Statistics, The Ohio State University, Columbus, OH 43210, USA

^acbdavis33@gmail.com; ^bhans@stat.osu.edu; ^csantner.1@osu.edu

Abstract

This research proposes a flexible Bayesian extension of the composite Gaussian process (CGP) model of Ba and Joseph (2012) for predicting (stationary or) non-stationary $y(\mathbf{x})$. The CGP generalizes the regression plus stationary Gaussian process (GP) model by replacing the regression term with a GP. The new model, $Y(\mathbf{x})$, can accommodate large-scale trends estimated by a global GP, local trends estimated by an independent local GP, and a third process to describe heteroscedastic data in which $Var(Y(\mathbf{x}))$ can depend on the inputs. This paper proposes a prior which ensures that the fitted global mean is smoother than the local deviations, and extends the covariance structure of the CGP to allow for differentially-weighted global and local components. A Markov chain Monte Carlo algorithm is proposed to provide posterior estimates of the parameters, including the values of the heteroscedastic variance at the training and test data locations. The posterior distribution is used to make predictions and to quantify the uncertainty of the predictions using prediction intervals. The method is illustrated using both stationary and non-stationary $y(\mathbf{x})$.

KEY WORDS: Composite Gaussian process model; Emulator; Gaussian process interpolator; Integrated mean squared prediction error; Uncertainty quantification; Universal kriging

1 Introduction

We introduce a Bayesian composite Gaussian process as a model for generating and predicting non-stationary functions $y(\mathbf{x})$ defined over an input space \mathcal{X} . Our model is motivated by and extends the work of Ba and Joseph (2012), who introduced a composite Gaussian process (CGP) as a flexible model for $y(\mathbf{x})$. They used $y(\mathbf{x})$ evaluations at training data locations $\mathbf{x}_i, i = 1, \dots, n$, to predict $y(\mathbf{x})$ at one or more new locations and to quantify uncertainty about these predictions.

The problem of predicting functions $y(\mathbf{x})$ that are possibly non-stationary is particularly relevant, as many physics-based and other simulator models have been developed as alternatives to physical experimental platforms. Termed “computer experiments”, simulator-based studies have been used, for example, to determine the engineering design of aircraft, automobiles, and prosthetic devices, to optimize the manufacturing settings of precision products by injection molding, and to evaluate public policy options (Ong *et al.*, 2008; Villarreal-Marroquín *et al.*, 2017; Lempert *et al.*, 2000).

A common approach to prediction and uncertainty quantification when analyzing data from a computer experiment is to represent the unknown function $y(\mathbf{x})$ as a realization of a Gaussian process (GP). As there are many possible functions that are consistent with the observed values $y(\mathbf{x}_i)$ sampled at training locations \mathbf{x}_i , a GP is used as a prior distribution over an infinite-dimensional space of functions. When combined with the observed data, the resulting posterior distribution over functions can be used for prediction and uncertainty quantification. The use of a GP as a prior over functions was introduced by O’Hagan (1978) in a Bayesian regression context. This approach has subsequently been extended and used extensively in various settings related to both physical and computer experiments (e.g., Sacks *et al.*, 1989; Neal, 1998; Kennedy and O’Hagan, 2001; Oakley, 2002; Banerjee *et al.*, 2004; Oakley and O’Hagan, 2004; Santner *et al.*, 2018).

Our interest lies in prediction and uncertainty quantification for functions that, when viewed as a draw from a GP, exhibit features inconsistent with stationarity, i.e. where the behavior of the function can be substantially different in different regions of the input space. Several existing methodologies exist for working with data generated by such functions. Perhaps the most widely-used is universal kriging (Cressie, 1993), which assumes the function $y(\mathbf{x})$ can be viewed as a draw from a GP of the form

$$Y(\mathbf{x}) = \sum_{j=1}^p f_j(\mathbf{x})\beta_j + Z(\mathbf{x}) = \mathbf{f}^\top(\mathbf{x})\boldsymbol{\beta} + Z(\mathbf{x}), \quad (1)$$

where $\mathbf{f}(\mathbf{x}) = (f_1(\mathbf{x}), \dots, f_p(\mathbf{x}))^\top$ is a vector of known regression functions, $\boldsymbol{\beta} = (\beta_1, \dots, \beta_p)^\top$ is a vector of unknown regression coefficients, and $Z(\mathbf{x})$ is a stationary Gaussian process with mean zero, process variance σ_Z^2 , and (positive definite) correlation function $R(\cdot)$ so that $Z(\mathbf{x})$ has

covariance

$$\text{Cov}(Z(\mathbf{x}), Z(\mathbf{x} + \mathbf{h})) = \sigma_Z^2 R(\mathbf{h}).$$

Throughout this paper the notation $Z(\mathbf{x}) \sim \text{GP}(0, \sigma_Z^2, R(\cdot))$ will be used to describe this stationary process assumption.

The intuition of the model is that $E(Y(\mathbf{x})) = \mathbf{f}^\top(\mathbf{x})\boldsymbol{\beta}$ describes large-scale $y(\mathbf{x})$ trends while $Z(\mathbf{x})$ describes small-scale deviations from the large-scale behavior. A special case of universal kriging is ordinary kriging which assumes $Y(\mathbf{x})$ has constant mean. Cressie (1993) and Santner *et al.* (2018) provide details about the model (1), including parametric options for $R(\mathbf{h})$, methods for estimating model parameters, prediction methodology for test data inputs, and uncertainty quantification of the predictions.

While universal kriging has proved useful in many applications, several limitations have been identified. The requirement that the regression functions be known or adaptively selected from a pre-defined collection of regression functions sometimes proves difficult. In addition to bias due to potential misspecification of the regression functions, standard prediction intervals under universal kriging do not account for uncertainty in the selection of the regression functions. From a computational perspective, entertaining a large class of potential regression functions may result in a large selection problem, necessitating a combinatorial search over a large space. Finally, the kriging methods described above are based on trend-stationary Gaussian processes. In many applications, even if the mean function is appropriate, the unknown function being emulated may exhibit non-stationary behavior due to the variance function. Ignoring these aspects of the data may result in both poor prediction and inaccurate uncertainty quantification.

As a motivating example, consider the (non-stationary) function

$$y(x) = \sin(30(x - 0.9)^4) \cos(2(x - 0.9)) + \frac{(x - 0.9)}{2}, \quad x \in [0, 1], \quad (2)$$

which was originally considered by Xiong *et al.* (2007) and also by Ba and Joseph (2012) (we henceforth refer to (2) as the BJX function). Figure 1 plots the BJX function as a black line. The points in the figure indicate the value of the function at the $n = 17$ training data locations used by Ba and Joseph (2012). If viewed as a realization of a stochastic process, one might describe the

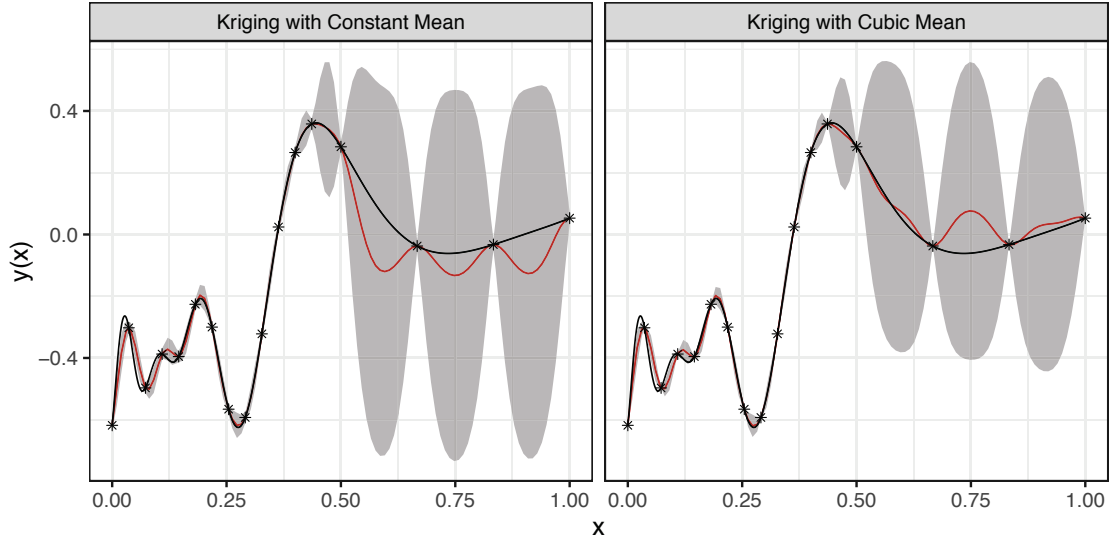


Figure 1: Kriging predictors (red lines) for the BJX function (black lines) given in equation (2) based on the training data shown as black points together with 95% prediction intervals. Left Panel: constant mean; Right Panel: cubic mean.

BJX function as having three behavior paradigms. For small x , $y(x)$ can be described as having a relatively flat global trend with rapidly-changing local adjustments. For intermediate x , $y(x)$ increases rapidly and smoothly, with few local departures. For large x , $y(x)$ has a relatively flat global trend with minor local adjustments.

Two aspects of universal kriging (UK) prediction of the BJX function are of interest: the accuracy of the point predictions and the narrowness of the associated uncertainty band. Figure 1 shows point predictions of $y(x)$ for the constant- and cubic-mean UK predictors computed at a 0.01 grid of prediction locations; a nugget was not included and so the predictors interpolate at the 17 training data locations. While the constant- and cubic-mean predictors and uncertainty bands are similar for $x < 0.5$, differences can be seen when $x > 0.5$. Reversion to the global mean is evident for the constant-mean predictor, while the cubic-mean predictor exhibits a “bump” near $x = 0.75$ that is driven by reversion to the estimated cubic mean function. The 95% prediction intervals based on the cubic mean are shorter than those based on the constant mean, however both sets of intervals are unreasonably wide when $x > 0.5$. Intuitively, the intervals should be short where $y(x)$ is essentially flat.

To address these shortcomings, alternatives to universal kriging have been proposed. The treed

Gaussian processes (TGPs) of Gramacy and Lee (2008) are one such alternative. The TGP model assumes that the input space can be partitioned into rectangular subregions so that a GP with a linear trend and stationary covariance structure is appropriate to describe $y(\mathbf{x})$ in each region. Following Breiman *et al.* (1984), TGP methodology partitions the input space by making binary splits on a sequence of the input variables over their ranges, where splits can be made on previously-split inputs by using a subregion of the previous range. After the input space is partitioned, the data in each region are used to fit a prediction model independently of the fits for other regions. In earlier proposals for fitting data to each region, Breiman *et al.* (1984) fit a constant mean model to the data in each region, and Chipman *et al.* (1998) fit a Bayesian hierarchical linear model in each region. The TGP model extends Chipman *et al.* (1998) by fitting a GP with a linear trend and stationary covariance structure in each region. While TGP prediction can have computational advantages over kriging, one disadvantage is that the method can be numerically challenged when the number of training data locations in one or more regions is small, a situation often encountered in computer experiments.

Ba and Joseph (2012) provide another alternative to universal kriging for emulating functions exhibiting non-stationary behavior. Their composite Gaussian process (CGP) avoids specification and/or selection of regression functions that might be required to generate the unknown $y(\mathbf{x})$ by specifying the generating GP $Y(\mathbf{x})$ as the sum

$$Y(\mathbf{x}) = Z_G(\mathbf{x}) + \sigma(\mathbf{x})Z_L(\mathbf{x}),$$

where, conditionally on model parameters $\mathbf{\Lambda}_{\text{CGP}}$, $Z_G(\mathbf{x})$ and $Z_L(\mathbf{x})$ are independent GPs such that

$$Z_G(\mathbf{x}) \mid \mathbf{\Lambda}_{\text{CGP}} \sim \text{GP}(\beta_0, \sigma_G^2, G(\cdot)) \quad \text{and} \quad Z_L(\mathbf{x}) \mid \mathbf{\Lambda}_{\text{CGP}} \sim \text{GP}(0, 1, L(\cdot)).$$

Under this specification, $Z_G(x)$ represents a smooth process that captures any global trend in $y(\mathbf{x})$, and $Z_L(\mathbf{x})$ represents a less-smooth process that introduces local adjustments to capture the function $y(\mathbf{x})$. By replacing the regression term in (1) with the more flexible $Z_G(\mathbf{x})$ process, the CGP model $Y(\mathbf{x})$ is able to adapt to large-scale global features of $y(\mathbf{x})$.

Ba and Joseph (2012) employ Gaussian correlation functions $G(\mathbf{h} \mid \boldsymbol{\rho}_G) = \prod_{j=1}^d \rho_{G,j}^{h_j^2}$ and $L(\mathbf{h} \mid$

$\boldsymbol{\rho}_L) = \prod_{j=1}^d \rho_{L,j}^{h_j^2}$ for the global and local processes, respectively, where $\boldsymbol{\rho}_G = (\rho_{G,1}, \dots, \rho_{G,d})^\top$ and $\boldsymbol{\rho}_L = (\rho_{L,1}, \dots, \rho_{L,d})^\top$ are corresponding correlation parameters. To ensure that the global process is smoother than the local process—and hence is interpretable as a global trend—a vector of positive bounds \mathbf{b} is specified so that $0 \leq \rho_{L,j} \leq b_j \leq \rho_{G,j} \leq 1$, $j = 1, \dots, d$. Even though the conditional process mean, $E(Y(\mathbf{x}) \mid \mathbf{A}_{\text{CGP}}) = \beta_0$, is constant across the input space, the examples in Ba and Joseph (2012) and that of the BJX function below show that CGP often has greater prediction accuracy than ordinary kriging or even universal kriging (when the global trend is difficult to capture with pre-specified regression functions).

The variance of the CGP $Y(\mathbf{x})$ is $\text{Var}(Y(\mathbf{x}) \mid \mathbf{A}_{\text{CGP}}) = \sigma_G^2 + \sigma^2(\mathbf{x})$. The term $\sigma(\mathbf{x})$ is a positive function that allows the range of the local process $Y_L(\mathbf{x})$, and hence the range of $Y(\mathbf{x})$, to vary over the input space. Ba and Joseph (2012) describe an algorithm for estimating $\sigma^2(\mathbf{x})$ that is implemented in their R package CGP (Ba and Joseph, 2018).

Figure 2 plots CGP predictions of the BJX test function (2) based on the same $n = 17$ run training data as above. For this example, the CGP predictions are clearly more accurate across the input space than predictions under both kriging approaches shown in Figure 1. The global predictor is smooth and captures the overall trend of the function well. When the data are less volatile, as over the range $x \in [0.4, 1]$, the global predictor essentially interpolates the data, and the local predictions are approximately zero. Comparing uncertainty quantification between the methods, for small x , CGP produces intervals that appear slightly wider than the intervals under both kriging approaches. The CGP interval widths for large x appear to fall in between the interval widths for kriging with constant and cubic mean functions, and indicate a large amount of uncertainty about the function in a region where it is essentially flat.

This paper introduces a Bayesian composite Gaussian process (BCGP) model that modifies and extends the CGP model in several ways. The BCGP model extends the covariance structure used by Ba and Joseph (2012) to allow the global and local correlation functions to be differentially weighted. This provides the covariance function with greater flexibility to handle data sets where more or less local adaptation is required. An additional feature of the BCGP model is that it introduces a new, flexible approach for handling the variance function $\sigma^2(\mathbf{x})$. Direct modeling of the latent variance process is straightforward in the Bayesian context as it simply requires a new

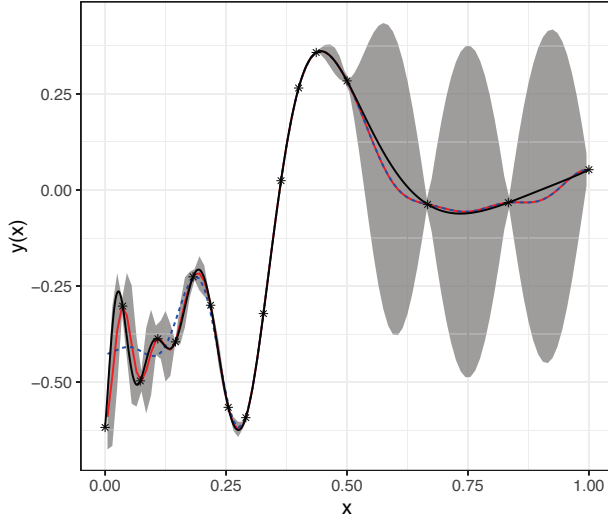


Figure 2: Predictions (in red) of the BJJ test function $y(\mathbf{x})$ in (2) and associated 95% uncertainty intervals (as a gray shadow) based on the CGP model. The dashed blue line is the estimate of the global component $Y_G(\mathbf{x})$ under the CGP model.

level in a hierarchical model and an additional step in a Markov chain Monte Carlo algorithm. We believe this direct approach to modeling will result in more accurate representations of uncertainty and will provide the model with additional flexibility for adapting to situations where the range of $y(\mathbf{x})$ varies significantly across the input space. More generally, by formulating the model in a Bayesian context we are able to quantify uncertainty in the unknown model parameters. By fully integrating over the unknown parameters to predict $y(\mathbf{x})$, the methodology allows one to fully quantify uncertainty in the predicted values.

After the BCGP model is introduced in Section 2, Section 3 describes the computational algorithm we have developed for prediction and uncertainty quantification. Section 4 performs prediction and uncertainty quantification for three examples. The first example is the BJJ example, the second example is a $d = 4$ setting that, visually, appears stationary, and the third example performs prediction for a $d = 10$ analytic example of the wing weight of a light aircraft.

2 The Bayesian Composite Gaussian Process Model

This section describes a Bayesian composite Gaussian process (BCGP) model that can be used to predict functions $y(\mathbf{x})$, $\mathbf{x} \in \mathcal{X}$, that, when viewed as a draw from a stochastic process, exhibit

behavior consistent with non-stationarity. We assume that (perhaps after a suitable transformation) the input space \mathcal{X} is a d -dimensional, finite hyper-rectangle denoted by $[\mathbf{a}, \mathbf{b}]^d \equiv \prod_{j=1}^d [a_j, b_j]$, with $-\infty < a_j \leq x_j \leq b_j < +\infty$ for $j = 1, \dots, d$. As part of the model specification below, we extend the GP notation for stationary processes, $\text{GP}(\beta_0, \sigma_Z^2, R(\cdot))$, for use with nonstationary GPs by letting $Y(\mathbf{x}) \sim \text{GP}(\mu(\mathbf{x}), C(\cdot, \cdot))$ indicate that $Y(\mathbf{x})$ follows a Gaussian process with $E(Y(\mathbf{x})) = \mu(\mathbf{x})$ and covariance function $C(\cdot, \cdot)$. Throughout, we assume that the training data have been centered to have mean zero and scaled to have unit variance.

2.1 Conditional Model

The conditional (likelihood) component of the BCGP model assumes that $y(\mathbf{x})$ can be viewed as a realization from a random process $Y(\mathbf{x})$ that can be decomposed as

$$Y(\mathbf{x}) = Y_G(\mathbf{x}) + Y_L(\mathbf{x}) + \epsilon(\mathbf{x}), \quad \mathbf{x} \in [\mathbf{a}, \mathbf{b}]^d, \quad (3)$$

where $Y_G(\mathbf{x})$, $Y_L(\mathbf{x})$ and $\epsilon(\mathbf{x})$ are mutually independent Gaussian processes. As in the CGP of Ba and Joseph (2012), the decomposition includes a global component, $Y_G(\mathbf{x})$, and a local deviation component, $Y_L(\mathbf{x})$. However, as seen below, our model specification differs in significant ways. First, the model allows for the possible inclusion of a measurement error or nugget process $\epsilon(\mathbf{x})$ (see Gramacy and Lee, 2012, for a detailed discussion of the use of a nugget term in GP models for computer simulator output). Ba and Joseph (2012) argue that, due to the formulation of their CGP, the local process may mimic a nugget term in some situations and hence do not include such a term explicitly. We recognize that different practitioners will have different views on inclusion of a nugget component and note that, while we have formulated the BCGP model to include the $\epsilon(\mathbf{x})$ for completeness, the nugget component can be easily removed if desired.

Conditional on model parameters $\mathbf{\Lambda} = (\beta_0, \omega, \boldsymbol{\rho}_G, \boldsymbol{\rho}_L, \sigma_\epsilon^2, \sigma^2(\cdot))$, we assume $Y_G(\mathbf{x}) \mid \mathbf{\Lambda} \sim \text{GP}(\beta_0, C_G(\cdot, \cdot))$, where

$$C_G(Y_G(\mathbf{x}_s), Y_G(\mathbf{x}_t)) = \begin{cases} \sigma(\mathbf{x}_s)\sigma(\mathbf{x}_t)\omega G(\mathbf{x}_s - \mathbf{x}_t \mid \boldsymbol{\rho}_G) & , \mathbf{x}_s \neq \mathbf{x}_t, \\ \sigma^2(\mathbf{x}_s)\omega & , \mathbf{x}_s = \mathbf{x}_t, \end{cases} \quad (4)$$

$\sigma(\mathbf{x})$ is a positive function, G is a global correlation function, and $\omega \in [0, 1]$ is a weight. The local process is specified as $Y_L(\mathbf{x}) \mid \mathbf{\Lambda} \sim GP(0, C_L(\cdot, \cdot))$, where

$$C_L(Y_L(\mathbf{x}_s), Y_L(\mathbf{x}_t)) = \begin{cases} \sigma(\mathbf{x}_s)\sigma(\mathbf{x}_t)(1 - \omega)L(\mathbf{x}_s - \mathbf{x}_t \mid \boldsymbol{\rho}_L) & , \mathbf{x}_s \neq \mathbf{x}_t, \\ \sigma^2(\mathbf{x}_s)(1 - \omega) & , \mathbf{x}_s = \mathbf{x}_t, \end{cases} \quad (5)$$

and L is a local correlation function. The process $\epsilon(\mathbf{x})$ is a mean zero Gaussian white noise process with variance σ_ϵ^2 .

The functions G and L are taken to be the Gaussian correlation functions

$$G(\mathbf{h} \mid \boldsymbol{\rho}_G) = \prod_{j=1}^d \rho_{G,j}^{K_G(h_j)^2}, \text{ and } L(\mathbf{h} \mid \boldsymbol{\rho}_L) = \prod_{j=1}^d \rho_{L,j}^{K_L(h_j)^2} \quad (6)$$

with unknown parameters $\boldsymbol{\rho}_G = (\rho_{G,1}, \dots, \rho_{G,d})$ and $\boldsymbol{\rho}_L = (\rho_{L,1}, \dots, \rho_{L,d})$. The quantities K_G and K_L are positive constants selected to enhance the numerical stability of operations on the correlation matrices of the data; the values $K_G = K_L = 16$ are often appropriate when the data have been scaled to have unit variance. As with the CGP model, we take $Y_G(\mathbf{x})$ to be a smooth process that captures any global trend of $y(\mathbf{x})$, while $Y_L(\mathbf{x})$ adapts to local deviations. The relative smoothness of draws from $Y_G(\mathbf{x})$ and $Y_L(\mathbf{x})$ is controlled by the global and local correlation parameters $\boldsymbol{\rho}_G$ and $\boldsymbol{\rho}_L$. We force $Y_G(\mathbf{x})$ to be smoother than $Y_L(\mathbf{x})$ by embedding constraints in the joint prior distribution for $\boldsymbol{\rho}_G$ and $\boldsymbol{\rho}_L$.

Conditional on $\mathbf{\Lambda}$, the $Y(\mathbf{x})$ process (3) can be equivalently specified as

$$Y(\mathbf{x}) \mid \mathbf{\Lambda} \sim GP(\beta_0, C(\cdot, \cdot)), \mathbf{x} \in [\mathbf{a}, \mathbf{b}]^d, \quad (7)$$

where β_0 is the overall mean, and

$$C(Y(\mathbf{x}_s), Y(\mathbf{x}_t)) = \begin{cases} \sigma(\mathbf{x}_s)\sigma(\mathbf{x}_t) (\omega G(\mathbf{x}_s - \mathbf{x}_t \mid \boldsymbol{\rho}_G) + (1 - \omega) L(\mathbf{x}_s - \mathbf{x}_t \mid \boldsymbol{\rho}_L)) & , \mathbf{x}_s \neq \mathbf{x}_t, \\ \sigma^2(\mathbf{x}_s) + \sigma_\epsilon^2 & , \mathbf{x}_s = \mathbf{x}_t. \end{cases} \quad (8)$$

The specification in (3)-(5) emphasizes the decomposition of the process into global, local and error components, while the specification in (7)-(8) emphasizes the roles of the parameters in the overall

covariance function.

As noted in Section 2.1, the parameters $\boldsymbol{\rho}_G$ and $\boldsymbol{\rho}_L$ control the smoothnesses of the component processes in $C(Y(\cdot), Y(\cdot))$. The parameter ω determines the extent that the model can make local adaptations to the global process; no local adaption is allowed when $\omega = 1$. The final $C(Y(\cdot), Y(\cdot))$ parameter is $\sigma(\mathbf{x})$. From (8), $\text{Var}(Y(\mathbf{x}) \mid \mathbf{\Lambda}) = \sigma^2(\mathbf{x}) + \sigma_\epsilon^2$. In the applications we consider, σ_ϵ^2 is typically small relative to the overall range of $y(\mathbf{x})$, and hence $\sigma^2(\mathbf{x})$ plays the critical role in prediction and uncertainty quantification with respect to the model variance. The conditional BCGP model relies on knowing the form of $\sigma^2(\mathbf{x})$, which is typically not available in practice. Rather than defining an algorithm for estimating $\sigma^2(\mathbf{x})$ as in Ba and Joseph (2012), we propose to model directly this function as an unknown random function by assuming

$$\log \sigma^2(\mathbf{x}) \mid \mu_V, \sigma_V^2, \boldsymbol{\rho}_V \sim \text{GP}(\mu_V, \sigma_V^2, G(\cdot \mid \boldsymbol{\rho}_V)), \quad (9)$$

where $G(\cdot \mid \boldsymbol{\rho}_V)$ is the Gaussian correlation function in (6) with parameters $\boldsymbol{\rho}_V$.

Modeling the variance function as a latent process provides a model-based approach for flexibly estimating the volatility of the unknown function $y(\mathbf{x})$ across the input space. Specification of the model in this way introduces new, low-level parameters μ_V , σ_V^2 and $\boldsymbol{\rho}_V$ that drive the unobserved process. Our model for the variance process is easily handled in our inferential and predictive framework for two reasons. First, because we use MCMC methods for inference and prediction, the fact that the variance process is simply a level in a Bayesian hierarchical model means that values of $\sigma^2(\mathbf{x})$ and of the hyper-parameters of this latent process can be updated by additional sampling steps. Second, due to the initial scaling of the data, it is possible to use a prior distribution to center the parameters of the log Gaussian process around reasonable values. This allows us to anchor the $\sigma^2(\mathbf{x})$ function along a plausible trajectory while giving it the freedom to adapt to information contained in the training data.

2.2 Prior Model

We complete the specification of the BCGP model with a prior distribution on the unknown model parameters $\mathbf{\Lambda}$ that factorizes as follows:

$$p(\beta_0) p(\omega) p(\sigma_\epsilon^2) p(\mu_V) p(\sigma_V^2) \prod_{j=1}^d p(\rho_{L,j} | \rho_{G,j}) p(\rho_{G,j}) p(\rho_{V,j}). \quad (10)$$

As is common in the literature, we assume a flat, location-invariant prior, $p(\beta_0) \propto 1$, for the overall process mean. When the error process is included in the model, we assign a gamma prior distribution to its variance, $\sigma_\epsilon^2 \sim \text{Gamma}(a_\epsilon, b_\epsilon)$, parameterized so that $E(\sigma_\epsilon^2) = a_\epsilon b_\epsilon$. For data from a computer simulator we typically select the hyperparameters so that σ_ϵ^2 is, *a priori*, close to zero with high probability (see Section 4 for examples).

The global correlation parameters are assumed to be independent of each other with $\rho_{G,j} \sim \text{Beta}(\alpha_{G,j}, \beta_{G,j})$, for $j = 1, \dots, d$. While in principle one could chose different hyperparameters for each input dimension, reflecting different *a priori* beliefs about the function along each input, in absence of such knowledge we typically set each $\alpha_{G,j}$ and $\beta_{G,j}$ equal to common values α_G and β_G . To enforce greater smoothness in the global process than in the local process in each dimension, we specify the prior for the local correlation parameter conditionally on the corresponding global parameter as a beta distribution truncated to the interval $(0, \rho_{G,j})$:

$$\rho_{L,j} | \rho_{G,j} \stackrel{\text{ind.}}{\sim} \text{TrBeta}(\alpha_{L,j}, \beta_{L,j}; 0, \rho_{G,j}), \quad j = 1, \dots, d,$$

The notation $X \sim \text{TrBeta}(\alpha, \beta; c, d)$ refers to a beta random variable truncated to the interval (c, d) which has density

$$p(x) = \frac{\Gamma(\alpha + \beta)}{\Gamma(\alpha)\Gamma(\beta)} \frac{(x - c)^{\alpha-1} (d - x)^{\beta-1}}{(d - c)^{\alpha+\beta-1}}, \quad c \leq x \leq d,$$

with mean $E(X) = c + \left(\frac{\alpha}{\alpha+\beta}\right) (d - c)$ and variance $\text{Var}(X) = \frac{\alpha\beta(d-c)^2}{(\alpha+\beta)^2(\alpha+\beta+1)}$. Lacking substantive prior information about the parameters $\alpha_{L,j}$ and $\beta_{L,j}$ of $\rho_{L,j}$ we typically use common values α_L and β_L across the d inputs.

The prior for the parameter that weights the global and local correlation functions is taken to be $\omega \sim \text{TrBeta}(\alpha_\omega, \beta_\omega; L_\omega, U_\omega)$, where $0 \leq L_\omega < U_\omega \leq 1$. Often the prior for ω is truncated with $L_\omega = 0.5$ and $U_\omega = 1$ to put more weight on the global process.

Finally, we assign a prior to the parameters $(\mu_V, \sigma_V^2, \rho_V)$ of the latent variable process $\sigma^2(\mathbf{x})$

in (9) to have mutually independent components with marginals

$$\mu_V \sim N(\beta_V, \tau_V^2), \quad \sigma_V^2 \sim \text{IG}(a_{\sigma_V^2}, b_{\sigma_V^2}), \quad \rho_{V,j} \stackrel{\text{iid}}{\sim} \text{Beta}(\alpha_{\rho_{V,j}}, \beta_{\rho_{V,j}}), \quad j = 1, \dots, d,$$

where $\text{IG}(a, b)$ represents the inverse gamma distribution with mean $(a - 1)^{-1}b^{-1}$ when $a > 1$. To specify values for the six hyper-parameters above recall that, ignoring the error variance σ_ϵ^2 , $\sigma^2(\mathbf{x})$ is the variance of the $Y(\mathbf{x})$ process. Assuming that the output $y(\mathbf{x})$ has been scaled to have zero sample mean and unit sample variance, we “center” our prior so that $\sigma^2(\mathbf{x}) \approx 1$ on average. Setting $\beta_V = -\frac{1}{10}$, $\tau_V^2 = \frac{1}{10}$, $a_{\sigma_V^2} = 2 + \sqrt{\frac{1}{10}}$, and $b_{\sigma_V^2} = \frac{100}{1 + \sqrt{\frac{1}{10}}}$ encourages the $\sigma^2(\mathbf{x})$ process to stay near unity on average while allowing the data to suggest regions of the input space where $\sigma^2(\mathbf{x})$ should be larger or smaller. Lastly, the hyperparameters $\alpha_{\rho_{V,j}}$ and $\beta_{\rho_{V,j}}$ can be chosen to control the smoothness of the latent variance process. In general, we expect this process to be fairly smooth, which suggests picking values that encourage high correlation. If there is a strong prior belief that the unknown $y(\mathbf{x})$ may be best modeled as a stationary process, then setting the $\alpha_{\rho_{V,j}}$ and the $\beta_{\rho_{V,j}}$ to ensure that the $\rho_{V,j}$ are close to 1, will encourage a (nearly) constant variance function. Setting $\alpha_{\rho_{V,j}} = \beta_{\rho_{V,j}} = 1$ gives a non-informative $\text{Unif}(0, 1)$ distribution.

3 Computational Algorithms for Inference and Prediction

This section describes the computational algorithms we have developed for inference and prediction under the BCGP model. Assume that the unknown function $y(\mathbf{x})$ has been sampled at n training data sites in the input space, denoted $\mathbf{x}_i, i = 1, \dots, n$, and $\mathbf{y} = (y(\mathbf{x}_1), \dots, y(\mathbf{x}_n))^\top$ is the associated vector of computed values of $y(\mathbf{x})$. To simplify notation, let $\mathbf{V} = (\sigma^2(\mathbf{x}_1), \dots, \sigma^2(\mathbf{x}_n))^\top$ be the random vector of unknown values of the variance process at the training data locations. We augment the collection of parameters $\mathbf{\Lambda}$ introduced in Section 2.1 to include all unknown quantities so that now $\mathbf{\Lambda} = (\beta_0, \omega, \boldsymbol{\rho}_G, \boldsymbol{\rho}_L, \sigma_\epsilon^2, \mathbf{V}, \mu_V, \boldsymbol{\rho}_V, \sigma_V^2)$. The posterior distribution of all unknown quantities $\mathbf{\Lambda}$ has density function $p(\mathbf{\Lambda} \mid \mathbf{y}) \propto p(\mathbf{y} \mid \mathbf{\Lambda})p(\mathbf{\Lambda})$, where $p(\mathbf{\Lambda})$ is the prior specified in Section 2.2. The likelihood $p(\mathbf{y} \mid \mathbf{\Lambda})$ is derived from the conditional model specified in (7) and (8), which implies that $\mathbf{y} \mid \mathbf{\Lambda} \sim N(\beta_0 \mathbf{1}, \mathbf{C})$, where the $n \times n$ covariance matrix \mathbf{C} has $(i, j)^{\text{th}}$ element,

$1 \leq i, j \leq n,$

$$C_{ij} = \sigma(\mathbf{x}_i) \sigma(\mathbf{x}_j) (\omega G(\mathbf{x}_i - \mathbf{x}_j \mid \boldsymbol{\rho}_G) + (1 - \omega)L(\mathbf{x}_i - \mathbf{x}_j \mid \boldsymbol{\rho}_L)) + \delta_{i,j} \sigma_\epsilon^2, \quad (11)$$

and $\delta_{i,j}$ is the Kronecker delta function.

The posterior density $p(\boldsymbol{\Lambda} \mid \mathbf{y})$ is difficult to compute in closed form. For inferential and predictive purposes, we obtain samples from the posterior via a Markov chain Monte Carlo (MCMC) algorithm. We update parameters and the \mathbf{V} values based on their full conditional distributions either by Gibbs updates—sampling directly from full conditional distributions—or by Metropolis–Hastings updates—sampling from proposal distributions and accepting or rejecting the proposed draws based on full conditional distributions. Some updates are relatively straightforward, while others—in particular, the update of the latent variance process \mathbf{V} —require special attention in order to ensure good mixing of the chain.

The MCMC algorithm starts at an initial value $\boldsymbol{\Lambda}^{[0]}$ and, at each iteration t , the elements of $\boldsymbol{\Lambda}$ are updated according to the 9 steps below. The chain can be initialized with any $\boldsymbol{\Lambda}^{[0]}$ satisfying $p(\boldsymbol{\Lambda}^{[0]} \mid \mathbf{y}) > 0$. For simplicity the following notation is used. At any step in the sampler during iteration t , the notation $\boldsymbol{\Lambda}^{[t]}$ represents a vector containing the newly-sampled values for any parameters that have already been updated in the (partial) sweep through the steps at iteration t . Similarly, for steps with Metropolis–Hastings updates, the notation $\boldsymbol{\Lambda}'$ should be understood to mean $\boldsymbol{\Lambda}^{[t]}$ where the parameters currently being updated are replaced with proposed values. For a generic parameter θ , the notation $\boldsymbol{\Lambda}_{-\theta}^{[t]}$ should be understood to be the up-to-date version of the parameter vector without component θ . Unless otherwise specified, for all proposal distributions used in Metropolis–Hastings updates, if the proposed value is θ' , the updated value is taken to be

$$\theta^{[t+1]} = \begin{cases} \theta' & \text{with probability } \min \left\{ 1, \frac{p(\boldsymbol{\Lambda}' \mid \mathbf{y})}{p(\boldsymbol{\Lambda}^{[t]} \mid \mathbf{y})} \right\}, \\ \theta^{[t]} & \text{with probability } 1 - \min \left\{ 1, \frac{p(\boldsymbol{\Lambda}' \mid \mathbf{y})}{p(\boldsymbol{\Lambda}^{[t]} \mid \mathbf{y})} \right\}. \end{cases} \quad (12)$$

In our MCMC algorithm, a Metropolis–Hastings update for a parameter θ relies on a *calibrated proposal width* Δ_θ to help ensure reasonable mixing of the chain. Section 3.2 provides details of the calibration scheme.

At iteration t in the MCMC algorithm, the parameters are updated according to the following steps.

Step 1: Update β_0 by sampling $\beta_0^{[t+1]}$ directly from its full conditional distribution,

$$\beta_0 \mid \mathbf{\Lambda}_{-\beta_0}^{[t]}, \mathbf{y} \sim \text{N} \left(\left(\mathbf{1}^\top \mathbf{C}^{[t]-1} \mathbf{1} \right)^{-1} \mathbf{1}^\top \mathbf{C}^{[t]-1} \mathbf{y}, \left(\mathbf{1}^\top \mathbf{C}^{[t]-1} \mathbf{1} \right)^{-1} \right),$$

where $\mathbf{1}$ is a vector of ones and $\mathbf{C}^{[t]}$ is the covariance matrix with elements (11) evaluated at the training data points \mathbf{x}_i using the parameters $\mathbf{\Lambda}_{-\beta_0}^{[t]}$.

Step 2: Update ω by proposing ω' from a $\text{Unif}(\omega^{[t]} - \Delta_\omega, \omega^{[t]} + \Delta_\omega)$ distribution and using (12) to determine the value of $\omega^{[t+1]}$.

Step 3: Update the global correlation parameters $\rho_{G,1}, \dots, \rho_{G,d}$ one-at-a-time (conditioning on the others) by proposing $\rho'_{G,j}$ from a $\text{Unif}(\rho_{G,j}^{[t]} - \Delta_{\rho_{G,j}}, \rho_{G,j}^{[t]} + \Delta_{\rho_{G,j}})$ distribution and using (12) to determine the value of each $\rho_{G,j}^{[t+1]}$.

Step 4: Update the local correlation parameters $\rho_{L,1}, \dots, \rho_{L,d}$ one-at-a-time (conditioning on the others) by proposing $\rho'_{L,j}$ from a $\text{Unif}(\rho_{L,j}^{[t]} - \Delta_{\rho_{L,j}}, \rho_{L,j}^{[t]} + \Delta_{\rho_{L,j}})$ distribution and using (12) to determine the value of each $\rho_{L,j}^{[t+1]}$.

Step 5: Update σ_ϵ^2 by proposing $\sigma_\epsilon'^2$ from a $\text{Unif}(\sigma_\epsilon^{2[t]} - \Delta_{\sigma_\epsilon^2}, \sigma_\epsilon^{2[t]} + \Delta_{\sigma_\epsilon^2})$ distribution and using (12) to determine the value of $\sigma_\epsilon^{2[t+1]}$.

Step 6: Update μ_V by sampling $\mu_V^{[t+1]}$ directly from its full conditional distribution,

$$\mu_V \mid \mathbf{\Lambda}_{-\mu_V}^{[t]}, \mathbf{y} \sim \text{N}(m, v),$$

where $v^{-1} = 1/\tau_V^2 + \mathbf{1}^\top \mathbf{R}_t^{[t]-1} \mathbf{1} / \sigma_V^{2[t]}$ and $m = v(\beta_V / \tau_V^2 + \mathbf{1}^\top \mathbf{R}_t^{[t]-1} \mathbf{W}^{[t]} / \sigma_V^{2[t]})$, $\mathbf{W}^{[t]} = \log \mathbf{V}^{[t]} = \left(\log \sigma^{2[t]}(\mathbf{x}_1), \dots, \log \sigma^{2[t]}(\mathbf{x}_n) \right)^\top$, and $\mathbf{R}_t^{[t]}$ is the correlation matrix for the $\log \sigma^2(\mathbf{x})$ process evaluated at the training data locations with elements

$$\mathbf{R}_{t_{ij}}^{[t]} = G \left(\mathbf{x}_i - \mathbf{x}_j \mid \rho_V^{[t]} \right).$$

Step 7: Update σ_V^2 by sampling $\sigma_V^{2[t+1]}$ directly from its full conditional distribution,

$$\sigma_V^2 \mid \mathbf{\Lambda}_{-\sigma_V^2}^{[t]}, \mathbf{y} \sim IG \left(\frac{n}{2} + a_{\sigma_K^2}, \left(\frac{1}{2} (\mathbf{W}^{[t]} - \mu_V^{[t+1]})^\top (\mathbf{R}_t^{[t]})^{-1} (\mathbf{W}^{[t]} - \mu_V^{[t+1]}) + \frac{1}{b_{\sigma_K^2}} \right)^{-1} \right).$$

Step 8: Update $\rho_{V,1}, \dots, \rho_{V,d}$ one-at-a-time (conditioning on the others) by proposing $\rho'_{V,i}$ from a $\text{Unif}(\rho_{V,i}^{[t]} - \Delta_{\rho_{V,i}}, \rho_{V,i}^{[t]} + \Delta_{\rho_{V,i}})$ distribution and using (12) to determine the value of each $\rho_{V,i}^{[t+1]}$.

Step 9: Update $\mathbf{V} = (\sigma^2(\mathbf{x}_1), \dots, \sigma^2(\mathbf{x}_n))^\top$ as described in Section 3.1.

In practice, the MCMC algorithm is run for three sets of iterations. The first set are *calibration* iterations in which a fixed number of iterations are made in which the proposal widths Δ_θ are determined for the subsequent runs (see Section 3.2). After calibration, the chain is run for an additional *burn-in* period. The final set of iterations are *n_{mcmc} production* iterations that produce samples $\mathbf{\Lambda}^{[1]}, \dots, \mathbf{\Lambda}^{[n_{mcmc}]}$ from the posterior distribution $p(\mathbf{\Lambda} \mid \mathbf{y})$. The samples can be used for predictive inference as described in Section 3.3.

3.1 Updating the latent variance process \mathbf{V}

Updating the latent variance process at the training data locations $\mathbf{x}_1, \dots, \mathbf{x}_n$ requires special attention. The full conditional posterior distribution of neither \mathbf{V} nor its logarithm, \mathbf{W} , are standard distributions and so sampling updated values directly is difficult. When the number of training data locations, n , is not “too large”, we can use a Metropolis–Hastings update for the full vector \mathbf{V} by sampling from a proposal process at the training data locations and accepting the proposed move with the appropriate probability. While straightforward in principle, the proposal process must be constructed carefully in order to ensure acceptance rates that result in appropriate mixing of the chain. When n is large it is difficult to accept the entire vector of proposed values \mathbf{V}' unless the proposal vector is very close to the current vector, which inhibits mixing.

With this in mind, we describe two different methods for updating the latent variance process. The first method is designed to work well when n is “small”, while the second method is constructed to produce reasonable mixing when n is large. When the number of training data locations is small,

say $n < 20$, we recommend updating \mathbf{V} by sampling

$$\mathbf{W}' \sim N\left(\mathbf{W}^{[t]}, \mathbf{K}_W^{[t]}\right), \quad (13)$$

where $\mathbf{W}^{[t]} = \log \mathbf{V}^{[t]} = \left(\log \sigma^{2[t]}(\mathbf{x}_1), \dots, \log \sigma^{2[t]}(\mathbf{x}_n)\right)^\top$, $\mathbf{K}_{W_{ij}}^{[t]} = \tau^2 G\left(\mathbf{x}_i - \mathbf{x}_j \mid \boldsymbol{\rho}_V^{[t+1]}\right)$, and τ^2 is a predefined value that controls the variance of the proposal distribution. The proposal distribution (13) is centered around the current value at each training data location. The variance parameter τ^2 should be chosen so that the proposed values, \mathbf{W}' , are (1) similar enough to the current values, $\mathbf{W}^{[t]}$, to have a useful acceptance rate while (2) still allowing the \mathbf{W}' to be sufficiently different from the $\mathbf{W}^{[t]}$ values so the support of the posterior distribution can be fully explored. After appropriately accounting for the transformation, the acceptance probability for the proposed value $\mathbf{V}' = (e^{W'_1}, \dots, e^{W'_n})^\top$ is $\min\{1, p\}$, where

$$p = \frac{p(\mathbf{y} \mid \boldsymbol{\Lambda}')}{p(\mathbf{y} \mid \boldsymbol{\Lambda}^{[t]})} \times \frac{\exp\left(-\frac{1}{2}\left(\mathbf{W}' - \mu_V^{[t+1]}\mathbf{1}\right)^\top \mathbf{K}^{[t]-1}\left(\mathbf{W}' - \mu_V^{[t+1]}\mathbf{1}\right)\right)}{\exp\left(-\frac{1}{2}\left(\mathbf{W}^{[t]} - \mu_V^{[t+1]}\mathbf{1}\right)^\top \mathbf{K}^{[t]-1}\left(\mathbf{W}^{[t]} - \mu_V^{[t+1]}\mathbf{1}\right)\right)}. \quad (14)$$

When the number of training data locations is large, say $n \geq 20$, we recommend an alternate approach to updating \mathbf{V} . Rather than updating all n elements of \mathbf{V} together, we instead randomly select a focal point from the design space and then update the variance process at a cluster of n_{prop} training locations closest to the chosen focal point conditionally on the current value of the variance process at all other training data locations. After updating the process at that cluster of points, we randomly select another focal point in the design space and repeat the process. At each iteration in the overall MCMC algorithm, the process is repeated so that m total focal points are sampled, and the final vector \mathbf{V} after the m cycles is retained as new state $\mathbf{V}^{[t+1]}$ in the Markov chain. While $m = 1$ yields a valid MCMC algorithm, we expect setting $m > 1$ should improve mixing of the chain. The following steps describe the details of this process.

Step 9a: Select a focal point uniformly at random from the d -dimensional, hyper-rectangular input space $[\mathbf{a}, \mathbf{b}]^d$.

Step 9b: Select the n_{prop} training data locations closest to the randomly selected focal point. In practice, we have found that choosing $n_{prop} = 15$ works well. Denote these points by $\bar{\mathbf{x}}$ and

the remaining training data points by $\underline{\mathbf{x}}$.

Step 9c: Propose new values $\mathbf{W}'(\bar{\mathbf{x}})$ by sampling from the distribution obtained by conditioning (13) on the current values $\mathbf{W}^{[t]}(\underline{\mathbf{x}})$:

$$\mathbf{W}'(\bar{\mathbf{x}}) \mid \mathbf{W}^{[t]}(\underline{\mathbf{x}}), \boldsymbol{\rho}_V^{[t+1]} \sim \text{N} \left(\mathbf{W}^{[t]}(\bar{\mathbf{x}}), \tau^2 \left(\mathbf{R}_{\bar{\mathbf{W}}} - \mathbf{R}_{\bar{\mathbf{W}}, \underline{\mathbf{W}}}^\top \mathbf{R}_{\underline{\mathbf{W}}}^{-1} \mathbf{R}_{\bar{\mathbf{W}}, \underline{\mathbf{W}}} \right) \right),$$

where $\mathbf{R}_{\bar{\mathbf{W}}_{ij}} = G \left(\bar{\mathbf{x}}_i - \bar{\mathbf{x}}_j \mid \boldsymbol{\rho}_V^{[t+1]} \right)$ is the $n_{prop} \times n_{prop}$ correlation matrix for the log GP between the proposal locations, $\mathbf{R}_{\underline{\mathbf{W}}_{ij}} = G \left(\underline{\mathbf{x}}_i - \underline{\mathbf{x}}_j \mid \boldsymbol{\rho}_V^{[t+1]} \right)$ is the $(n - n_{prop}) \times (n - n_{prop})$ correlation matrix for the log GP between the locations in $\underline{\mathbf{x}}$, and $\mathbf{R}_{\bar{\mathbf{W}}, \underline{\mathbf{W}}_{ij}} = G \left(\underline{\mathbf{x}}_i - \bar{\mathbf{x}}_j \mid \boldsymbol{\rho}_V^{[t+1]} \right)$ is an $(n - n_{prop}) \times n_{prop}$ matrix with each column containing the correlation for the log GP between a proposal point and each of the locations in $\underline{\mathbf{x}}$.

Step 9d : Update the elements of $\mathbf{W}^{[t]}$ corresponding to the locations $\bar{\mathbf{x}}$ with the values $\mathbf{W}'(\bar{\mathbf{x}})$ with probability $\min\{1, p\}$, where p is as in (14); otherwise, do not change $\mathbf{W}^{[t]}$.

Step 9e: After repeating Steps (9a)-(9d) m times, set $\mathbf{W}^{[t+1]} = \mathbf{W}^{[t]}$ and $\mathbf{V}^{[t+1]} = \exp \left(\mathbf{W}^{[t+1]} \right) = \left(\sigma^{2[t+1]}(\mathbf{x}_1), \dots, \sigma^{2[t+1]}(\mathbf{x}_n) \right)^\top$.

In our examples, we typically set m so that $m \times n_{prop} > n$, which has resulted in satisfactory mixing of the chain.

3.2 Calibrating the proposal widths

The Metropolis–Hastings updates described above rely on proposal widths Δ_ω , $\Delta_{\rho_{G,j}}$, $\Delta_{\rho_{L,j}}$, $\Delta_{\sigma_\epsilon^2}$ and $\Delta_{\rho_{V,j}}$. Appropriate values must be chosen in order to ensure good mixing of the chain. We use an automated method to calibrate these proposal widths with the goal of selecting widths that result in acceptance rates of between approximately 0.2 and 0.4. It has been shown theoretically that in specific contexts acceptance rates in this range lead to chains with good convergence and mixing properties (e.g., Gelman *et al.*, 1996; Roberts *et al.*, 1997; Roberts and Rosenthal, 2001); empirical evidence in many different model and data settings suggests these rates are generally desirable.

To adaptively calibrate the proposal widths, we initially run the MCMC algorithm with user-specified widths Δ_θ . The proposal widths can be different for each parameter w , $\rho_{G,j}$, *etc.* After

n_{adapt} iterations, we compute the empirical acceptance rates separately for each parameter with a proposal width and compare these acceptance rates to a range of target rates (our implementations uses the range $[0.25, 0.40]$). If any individual empirical rate $acceptRate$ is outside of this range the proposal width for that parameter is updated to be $\Delta_\theta := \Delta_\theta * acceptRate/c$, where c is a specific target rate. Under this scheme, a proposal width will be increased when the empirical acceptance rate is too high and decreased when too low relative to the target. After updating the Δ_θ , the MCMC algorithm is continued for another n_{adapt} iterations. The adaptation scheme is terminated after a total of $numUpdates$ adaptation periods. Section 4 provides examples of how we have implemented this approach in practice.

Because the transition kernel is potentially changing throughout the adaptation period, we discard all samples at the end of the $numUpdates$ adaptation periods and start a new MCMC run using the final state of the chain as the starting values $\mathbf{\Lambda}^{[0]}$ and fixing the calibration widths Δ_θ at their final values. As we do not assume that we start the chain from stationarity, we typically allow for an additional burn-in period before collecting production samples from the posterior.

3.3 Prediction and Uncertainty Quantification

A primary objective is to use the methodology to predict the output of a computer simulator (or other source) at new input values. Quantification of uncertainty about these predictions is also desired. Focusing on a particular (single) input location \mathbf{x}_* , predictive inference under the BCGP model is obtained via the posterior predictive distribution

$$p(y(\mathbf{x}_*) | \mathbf{y}) = \int p(y(\mathbf{x}_*) | \mathbf{y}, \mathbf{\Lambda}) p(\mathbf{\Lambda} | \mathbf{y}) d\mathbf{\Lambda},$$

where the unknown parameters are integrated over their “likely” values as specified by the posterior distribution. The point prediction is taken to be the posterior predictive mean $E(Y(\mathbf{x}_*) | \mathbf{y})$. Uncertainty about the unknown value of $y(\mathbf{x}_*)$ is quantified by a $(1 - \alpha) \times 100\%$ posterior predictive interval computed as lower and upper $\alpha/2$ percentiles of the posterior predictive distribution.

To compute the predictions, note that the conditional distribution of $Y(\mathbf{x}_*)$ given $\mathbf{\Lambda}$ and \mathbf{y} is

$$Y(\mathbf{x}_*) | \mathbf{\Lambda}, \mathbf{y} \sim N \left(\beta_0 + \mathbf{C}_*^\top \mathbf{C}^{-1} (\mathbf{y} - \beta_0 \mathbf{1}), \sigma^2(\mathbf{x}_*) + \sigma_\epsilon^2 - \mathbf{C}_*^\top \mathbf{C}^{-1} \mathbf{C}_* \right), \quad (15)$$

where \mathbf{C} is the covariance matrix at the training data locations with elements calculated as in (11) and $\mathbf{C}_* = (C_{*1}, \dots, C_{*n})^\top$ is the vector of covariances between the process at the prediction input \mathbf{x}_* and the process at the training input locations; these elements are

$$C_{*i} = \sigma(\mathbf{x}_*)\sigma(\mathbf{x}_i)(wG(\mathbf{x}_* - \mathbf{x}_i | \boldsymbol{\rho}_G) + (1 - w)L(\mathbf{x}_* - \mathbf{x}_i | \boldsymbol{\rho}_L)),$$

for $i = 1, \dots, n$. The conditional distribution (15) can be used to construct the Rao–Blackwellized Monte Carlo estimate

$$\widehat{E}(Y(\mathbf{x}_*) | \mathbf{y}) = \frac{1}{n_{mcmc}} \sum_{t=1}^{n_{mcmc}} \left(\beta_0^{[t]} + \mathbf{C}_*^{[t]\top} \mathbf{C}^{[t]-1} (\mathbf{y} - \beta_0^{[t]} \mathbf{1}) \right) \quad (16)$$

of $E(Y(\mathbf{x}_*) | \mathbf{y})$ using the posterior samples obtained with the MCMC algorithm, where quantities superscripted by $[t]$ are computed using the t -th draw of the parameters, $\boldsymbol{\Lambda}^{[t]}$.

Computing $\mathbf{C}_*^{[t]}$ requires the term $\sigma^{[t]}(\mathbf{x}_*)$, the square root of the t^{th} *a posteriori* sample of the latent variance function at \mathbf{x}_* . While the method for updating the latent variance process described in Section 3.1 produces samples of the latent variance process at the training data locations, it does not automatically produce samples at the prediction location. If the prediction location is known in advance, the approach described in Section 3.1 can be modified to include the prediction location together with the training data locations. The resulting $\sigma^{[t]}(\mathbf{x}_*)$ can be saved for prediction.

If the prediction location is not known before the MCMC algorithm is run, samples can be obtained after the end of the MCMC run by simulating from the appropriate conditional distribution. In more detail, letting $W_* = \log \sigma^2(\mathbf{x}_*)$, we have

$$W_* | \boldsymbol{\Lambda}, \mathbf{y} \sim N \left(\mu_V + \mathbf{R}_*^\top \mathbf{R}^{-1} (\mathbf{W}_t - \mu_V \mathbf{1}), \sigma_V^2 (1 - \mathbf{R}_*^\top \mathbf{R}^{-1} \mathbf{R}_*) \right), \quad (17)$$

where \mathbf{R} is the $n \times n$ correlation matrix of the latent log GP evaluated at the training data locations and has ij -th element $\mathbf{R}_{ij} = G(\mathbf{x}_i - \mathbf{x}_j | \boldsymbol{\rho}_V)$. The term \mathbf{R}_* is the $n \times 1$ vector of covariances between the latent log GP at \mathbf{x}_* and each of the training data inputs \mathbf{x}_i , i.e., $\mathbf{R}_{*i} = G(\mathbf{x}_* - \mathbf{x}_i | \boldsymbol{\rho})$, for $i = 1, \dots, n$. Each posterior sample $\boldsymbol{\Lambda}^{[t]}$, $t = 1, \dots, n_{mcmc}$, is used to generate a draw $W_*^{[t]}$ from (17); transforming $W_*^{[t]}$ yields $\sigma^{[t]}(\mathbf{x}_*)$ which is required to evaluate the vector $\mathbf{C}_*^{[t]}$ in (16).

Uncertainty about the unknown value of the function at the input \mathbf{x}_* is quantified via a $(1 -$

$\alpha) \times 100\%$ posterior predictive interval computed by finding the upper and lower $\alpha/2$ percentiles of the posterior predictive distribution. As discussed in Davis (2015), Rao–Blackwellized Monte Carlo estimates of these quantities are more difficult to compute than the Rao–Blackwellized point predictions described above. A computationally simpler approach is to obtain the percentiles required to construct the predictive intervals by first obtaining samples $Y^{[t]}(\mathbf{x}_*)$, $t = 1, \dots, n_{mcmc}$, from the conditional predictive distribution (15) using the $\mathbf{\Lambda}^{[t]}$ and $\sigma^{[t]}(\mathbf{x}_*)$ samples. Then, for example, the 2.5th and 97.5th percentiles of this set of samples are Monte Carlo estimates of the endpoints of the 95% posterior predictive interval. Note that averaging the samples $Y^{[t]}(\mathbf{x}_*)$ together would also produce a valid estimate of $E(Y(\mathbf{x}_*) | \mathbf{y})$; however, when computationally feasible, we prefer the less-noisy, Rao–Blackwellized approach.

The methods of prediction and uncertainty quantification described above are specific to a single new input location \mathbf{x}_* . Point-wise prediction and uncertainty quantification at several new input locations \mathbf{x}_{*k} , $k = 1, \dots, n_p$, is easily achieved by implementing the methods separately at each location.

3.3.1 Global and Local Components of Prediction

Ba and Joseph (2012) emphasized that predictions under the CGP model can be decomposed into *global* and *local* components. Decomposing predictions in this way allows one to visually assess how the behavior of the unknown function changes over the input space, e.g. by finding regions where large local adaptations are necessary.

Posterior predictions under the BCGP model can be similarly decomposed by rewriting the conditional posterior predictive mean (15) as

$$\begin{aligned} E(Y(\mathbf{x}_*) | \mathbf{\Lambda}, \mathbf{y}) &= \beta_0 + \mathbf{C}_*^\top \mathbf{C}^{-1}(\mathbf{y} - \beta_0 \mathbf{1}) \\ &= \beta_0 + \mathbf{C}_{G_*}^\top \mathbf{C}^{-1}(\mathbf{y} - \beta_0 \mathbf{1}) + \mathbf{C}_{L_*}^\top \mathbf{C}^{-1}(\mathbf{y} - \beta_0 \mathbf{1}) + \mathbf{C}_{\epsilon_*}^\top \mathbf{C}^{-1}(\mathbf{y} - \beta_0 \mathbf{1}). \end{aligned} \quad (18)$$

The representation in (18) is due to the fact that the process covariance between the training data locations and the prediction location can be decomposed into global, local and error components. The elements of the vector \mathbf{C}_{G_*} are computed using the global covariance function (4) and represent the global component of the covariance between $Y(\mathbf{x}_*)$ and $Y(\mathbf{x}_i)$, $i = 1, \dots, n$; \mathbf{C}_{L_*} is defined

similarly for the local component of the covariance function (5). The vector \mathbf{C}_{ϵ_*} corresponds to the “error” component of the model. All elements of this vector will be zero unless we are predicting at one of the training data locations, i.e. $\mathbf{x}_* = \mathbf{x}_k$ for some $k \in \{1, \dots, n\}$, in which case the k th element of the vector will be σ_ϵ^2 .

Using this decomposition, the BCGP predictor (16) that averages over the posterior distribution of the unknown parameters can be re-written as

$$\widehat{E}(Y(\mathbf{x}_*) | \mathbf{y}) = \frac{1}{n_{mcmc}} \sum_{t=1}^{n_{mcmc}} \left(\widehat{y}_G^{[t]}(\mathbf{x}_*) + \widehat{y}_L^{[t]}(\mathbf{x}_*) + \widehat{y}_\epsilon^{[t]}(\mathbf{x}_*) \right),$$

where $\widehat{y}_g(\mathbf{x}_*) = \beta_0 + \mathbf{C}_{G_*}^\top \mathbf{C}^{-1}(\mathbf{y} - \beta_0 \mathbf{1})$, $\widehat{y}_L(\mathbf{x}_*) = \mathbf{C}_{L_*}^\top \mathbf{C}^{-1}(\mathbf{y} - \beta_0 \mathbf{1})$, and $\widehat{y}_\epsilon(\mathbf{x}_*) = \mathbf{C}_{\epsilon_*}^\top \mathbf{C}^{-1}(\mathbf{y} - \beta_0 \mathbf{1})$ can be viewed as the global, local and error components of the overall prediction, respectively. The error component $\widehat{y}_\epsilon(\mathbf{x}_*)$ will be zero except when making a prediction at one of the training data locations.

4 Examples

This section applies BCGP prediction to three examples. The first is the BJX function introduced in Section 1. The second is a $d = 4$ example using the output of a heat exchange simulator code. The final example uses output from a $d = 10$ analytic function for the wing weight of a light aircraft.

Example 4.1 Consider BCGP prediction of the $d = 1$ non-stationary $y(x)$ of Ba and Joseph (2012) and Xiong *et al.* (2007) given by equation (2). Prediction and uncertainty quantification of $y(x)$ are based on the BCGP model with the prior form described in Section 2.2 and the following hyperparameter specifications. BCGP was run using $60,000 = 60 \times 1000$ iterations for calibration, followed by 4,000 burn-in iterations, and 5,000 production iterations. The ω prior was taken to be the *Beta*(4, 6) distribution truncated to $[0.5, 1.0]$ which yields an ω prior mean of 0.7 and prior standard deviation of 0.074. The prior for $\rho_{G,1} = \rho_G$ was *Beta*(1.0, 0.4). The conditional distribution of $\rho_{L,1} = \rho_L$ given ρ_G was taken to be *Beta*(1.0, 1.0) truncated to $[0, \rho_G]$. Thus the prior mean for ρ_G is $1/1.4 = 0.71$ while the conditional prior mean for ρ_L is $0.5 \times \rho_G$.

The BCGP predictor and associated 95% point-wise uncertainty bounds are shown in Figure 3. As desired and seen by visual inspection, the bounds for $x > 0.5$ are not greatly influenced by the

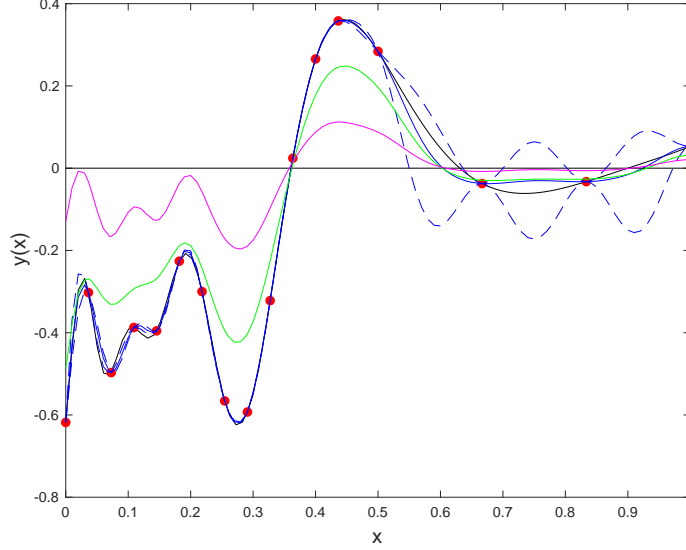


Figure 3: Prediction and 95% uncertainty bounds for the BJK function, $y(x)$, in Example 4.1 (solid black): the BCGP predictor of $y(x)$ (solid blue); 95% UQ limits of $y(x)$ (dashed blue); estimated posterior mean of the $Y_G(x)$ process (solid green); estimated posterior mean of the of the $Y_L(x)$ process (solid magenta).

relatively large variations in $y(x)$ for $x < 0.5$. In contrast, the 95% bands produced by kriging predictors having constant mean or cubic mean (Figure 1) contain a substantial amount of uncertainty when $x > 0.5$ that is caused by the stationarity assumption coupled by the training data with $x < 0.5$. Figure 3 also shows the posterior means of the predicted global and local deviations (and their sum, the predicted BJK function). The solid green global mean estimate, $\hat{y}_G(x)$, captures the global trend well and is not myopically concerned with the small variations in the function where $x < 0.5$. The solid purple local deviation estimate, $\hat{y}_L(x)$, is centered about zero and fluctuates more rapidly in regions where more adaptation is required. The sum of the two components produces the underlying $y(x)$.

Table 1 compares the prediction accuracy of the BCGP predictor with those of the kriging and

Predictor	RMSPE
Kriging/Constant mean	0.067
Kriging/Cubic mean	0.061
CGP	0.023
BCGP	0.014

Table 1: Root Mean Squared Prediction Errors (RMSPEs) over the grid $0.0(0.01)1.0$ for four predictors of the BJK function.

CGP predictors. While the BCGP predictor has the smallest root mean squared prediction error (RMSPE), the accuracy of the CGP predictor and BCGP predictor are comparable and about one half of that of the kriging predictors. In contrast, the uncertainty of the BCGP predictor as quantified by the 95% point-wise uncertainty bands is visually much smaller for the BCGP predictor than for any of the other three predictors. ■

Example 4.2 Qian *et al.* (2006) (see also Ba and Joseph, 2012) describe a computer simulation used in the design of a heat exchange system for electronic cooling applications. Denoted $y(\mathbf{x})$, the simulator output is the total rate of steady state heat transfer from the source, in this case an electronic device, to a sink which dissipates the heat. The $d = 4$ inputs to $y(\mathbf{x})$ are:

Notation	Description	Lower Bnd	Upper Bnd
x_1	Flow rate of entry air	0.00055	0.001
x_2	Temperature of entry air	270	303.15
x_3	Temperature of the heat source	330	400
x_4	Solid material thermal conductivity	202.4	360

Qian *et al.* (2006) provide computed steady state heat exchange values for 64 input vectors that form an orthogonal array-based Latin Hypercube design (Chap. 5 of Santner *et al.*, 2018). A design for the training data containing 40 inputs from among the 64 available was selected to (approximately) maximize the minimum interpoint distance; the remaining 24 inputs were used as test data. As suggested by the marginal plots of the training data shown in Figure 4, x_4 appears to be the most active input influencing $y(\mathbf{x})$ while x_2 also appears to be active but less so than x_4 . Figure 4 also suggests $y(\mathbf{x})$ appears to be well modeled as a draw from a linear regression plus stationary deviation process. This example will show that the BCGP model can predict $y(\mathbf{x})$ test data well in stationary deviation cases such as this appears to be.

As for Example 4.1, BCGP was run using $60,000 = 60 \times 1000$ iterations for calibration, followed by 4,000 burn-in iterations, and 5,000 production iterations; also, the ω prior was taken be the $Beta(4, 6)$ distribution truncated to $[0.5, 1.0]$. The prior for $\rho_{G,j}$, $j = 1, \dots, 4$, were taken to be independent and identically $Beta(1.0, 0.4)$ distributed. The conditional distribution of $\rho_{L,j}$ given $\rho_{G,j}$, $j = 1, \dots, 4$, were taken to have independent $Beta(1.0, 1.0)$ distributions truncated to $[0, \rho_{G,j}]$.

Draws from the posterior distribution of the model parameters are shown in Figure 5. The correlation parameters for the $Y_G(\mathbf{x})$ process, $\rho_{G,1}, \dots, \rho_{G,4}$, show that the inputs x_2 and x_4 appear

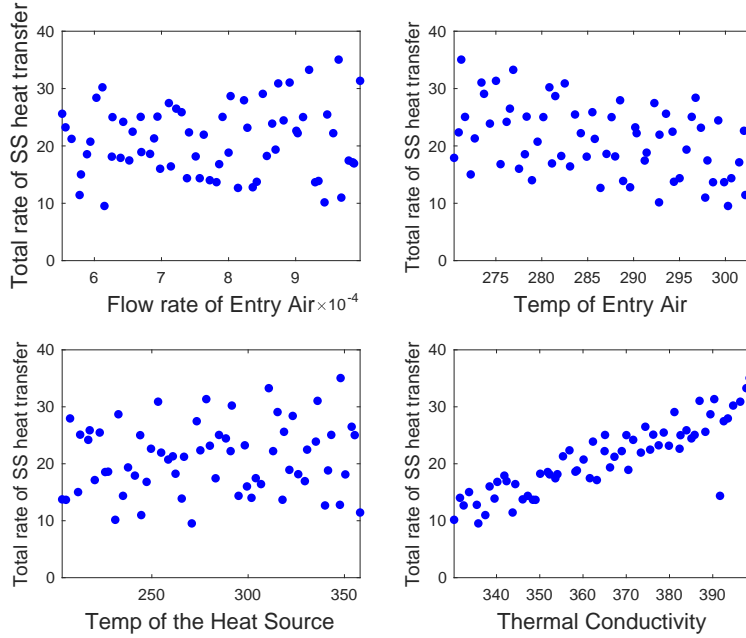


Figure 4: Marginal plots of state rate of heat transfer versus x_1, x_2, x_3, x_4 for Example 4.2.

most active because they have the smallest median draws, and the smaller $\rho_{G,4}$ values show that x_4 appears more active than x_2 . This is consistent with exploratory plots of the data in Figure 4. Also judging by the posterior correlation distributions, all four inputs are active for both the local deviation process $Y_L(\mathbf{x})$ and the $\sigma^2(\mathbf{x})$ process. Predicted surfaces for (the posterior means) of any of these processes can be displayed for sections of the input space that either fix 2 or more inputs or traverse a curve in 4-space

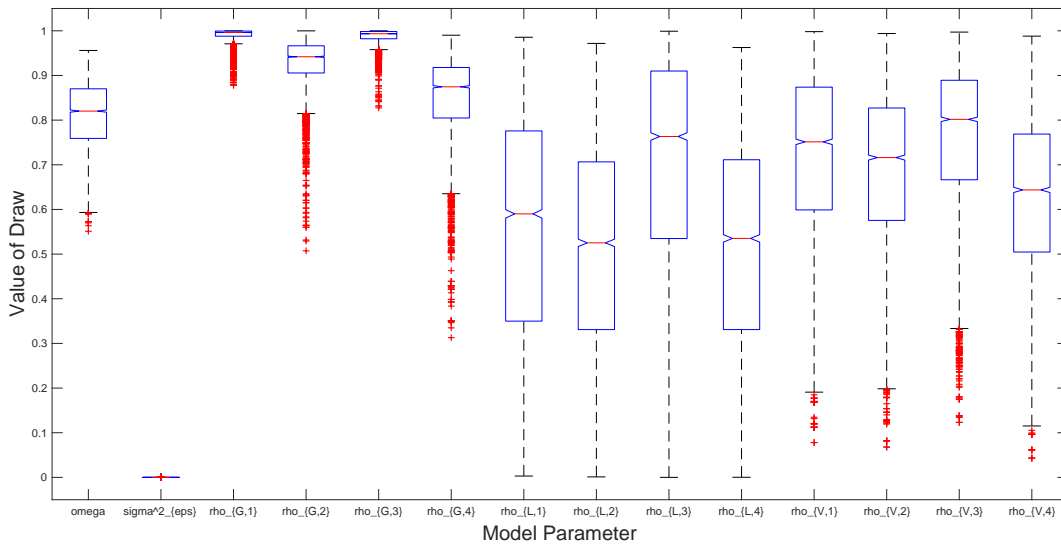


Figure 5: Boxplots of the posterior draws of all BCGP model parameters for Example 4.2

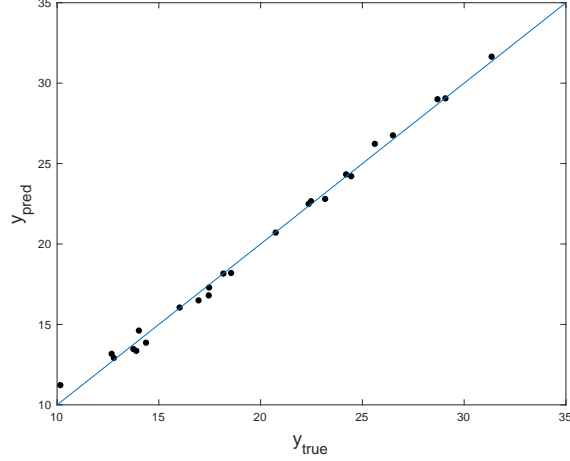


Figure 6: Predicted versus simulated values for the 24 steady state heat exchange inputs of Example 4.2

The posterior predictive mean of the $Y(\mathbf{x})$ process was estimated at the 24 test data locations. A plot of the simulated versus predicted values is shown in Figure 6 overlaid with the 45° line $y = x$. The predictions are, overall, extremely close to the true values and the RMSPE of the 24 predictions is 0.410. The predictive accuracy is similar to that of CGP (RMSPE equal to 0.438) and the kriging predictor with a linear mean (RMSPE equal to 0.480 when fit using REML with no nugget). These RMSPEs are about half that of the kriging predictor having a constant mean (RMSPE equal to 0.933 when fit using REML with no nugget). ■

Example 4.3 This final example contains a larger number of inputs, $d = 10$, than either Examples 4.1 or 4.2. Additionally the output model is analytic so one can easily test the prediction accuracy at arbitrary inputs. Forrester *et al.* (2008) state the equation

$$y(\mathbf{x}) = 0.036 S_w^{0.758} W_{wf}^{0.0035} \left(\frac{A}{\cos^2(\Lambda)} \right)^{0.6} q^{0.006} \lambda^{0.04} \left(\frac{100t_c}{\cos(\Lambda)} \right)^{-0.3} (N_Z W_{dg})^{0.49} + S_w W_p \quad (19)$$

for the weight of a light aircraft wing as a function of the 10 geometric/structural inputs with ranges provided in Table 2. Previous calculations of the *total sensitivity indices* for this $y(\mathbf{x})$ have shown that the most active inputs are, in order, $x_8 > x_3 > x_7 = x_1 > x_9$ and all other other inputs have only a minor impact.

The BCGP predictor was applied to $y(\mathbf{x})$ based on a 50 run input data set. A 50×10 run maximin Latin hypercube design having 10 inputs was selected as the input training data for predicting wing weight (<https://spacefillingdesigns.nl>). Then a 150×10 matrix of test data

Notation	Input (units)	Range
x_1/S_w	wing area (ft ²)	[150, 200]
x_2/W_{wf}	weight of fuel in the wing (lb)	[220, 300]
x_3/A	aspect ratio	[6, 10]
x_4/Λ	quarter-chord sweep (deg)	[-10, 10]
x_5/q	dynamic pressure at cruise (lb/ft ²)	[16, 45]
x_6/λ	taper ratio	[0.5, 1]
x_7/t_c	aerofoil thickness to chord ratio	[0.08, 0.18]
x_8/N_Z	ultimate load factor	[2.5, 6]
x_9/W_{dg}	flight design gross weight (lb)	[1, 700, 2, 500]
x_{10}/W_p	paint weight (lb/ft ²)	[0.025, 0.08]

Table 2: *Input variables and ranges for wing weight in Example 4.3.*

inputs was formed using the Sobol' sequence (Chap. 5 of Santner *et al.*, 2018). Prediction and uncertainty quantification of $y(x)$ are based on the BCGP model with prior as in Examples 4.1 and 4.2. In particular, the ω prior was the Beta(4, 6) distribution truncated to [0.5, 1.0] while the prior for each of the $d = 10$ global correlations, $\{\rho_{G,j}\}_{j=1}^{10}$, were given independent Beta(1, 0.4) distributions. The MCMC sampling used 60,000 = 60 × 1000 calibration iterations followed by a larger numbers of burn-in (5,000) and production iterations (10,000) for this larger d example than for Examples 4.1 and 4.2.

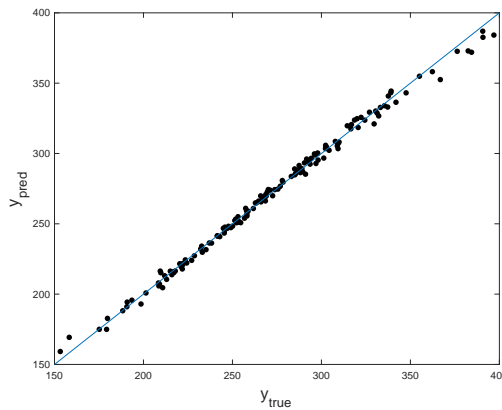


Figure 7: *Predicted wing weight versus calculated wing weight for 150 test inputs based on 50 training inputs from a maximin LHD.*

Figure 7 plots the 150 predicted wing weights versus the simulated wing weights from (19). The relative errors ranged from 1.1073×10^{-04} to 0.0694 and have mean 0.0097. To compare the

accuracy of the BCGP predictor with that of the CGP and two kriging predictors, the RMSPE for the 150 test inputs was calculated. The RMSPE for the BCGP predictor was 3.62, for the CGP predictor was 2.76, while that of the constant mean kriging predictor was 1.03, and that of the linear mean kriging predictor was 0.91. The kriging predictors are very accurate for this example.

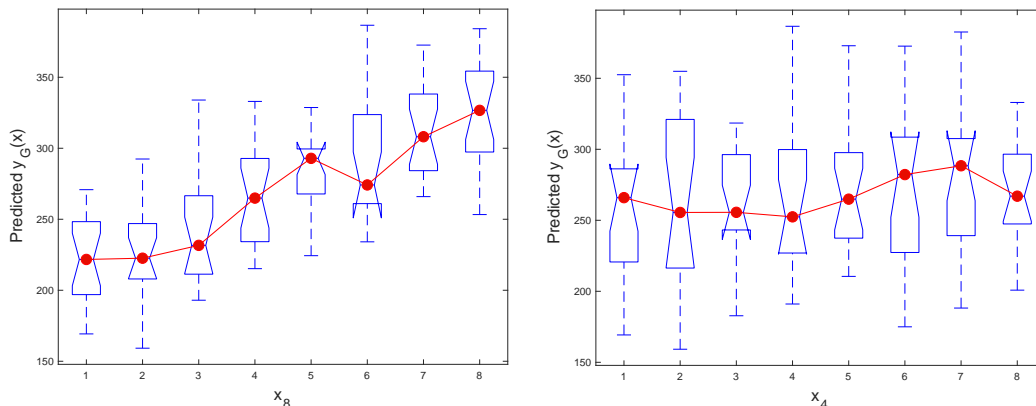


Figure 8: Boxplots of the predicted global trend function for the wing weight function, $\hat{y}_G(\mathbf{x})$, based on grouped x_8 and x_4 values for 150 test inputs.

One opportunity that CGP and BCGP provide is the opportunity to examine the *global trend* curve, $\hat{y}_G(\mathbf{x})$. Here we consider the activity of inputs on $\hat{y}_G(\mathbf{x})$. Recall that x_8 , x_3 , x_9 , were considered active for wing weight $y(\mathbf{x})$ while x_4 was considered in-/low-activity. It is natural to speculate that the same inputs are active or inactive for $y_G(\mathbf{x})$. To examine this question, fix $i \in \{1, \dots, 10\}$ and divide the range of x_i into 8 equal length subintervals. Then group the 150 predicted $y_G(\mathbf{x})$ into 8 groups according to the subinterval that x_i for that prediction falls. The grouped $y_G(\mathbf{x})$ predictions are plotted as 8 side-by-side boxplots in Figure 8. Connecting the medians of each boxplot shows that $y_G(\mathbf{x})$ increases in x_8 while the analogous plot for x_4 showed low $y_G(\mathbf{x})$ activity. Similar plots for x_3 , x_7 , x_1 , and x_9 show these inputs to be active while those for x_2 , x_5 , and x_6 show low activity. ■

5 Summary and Discussion

This paper proposes a Bayesian method to predict the output from a computer simulator that produces possibly non-stationary output $y(\mathbf{x})$. The methodology is developed to allow output containing measurement error. Based on a set of training data, prediction is based on a Bayesian Composite Gaussian process (BCGP) model $Y(\mathbf{x})$. The BCGP is a hierarchical $Y(\mathbf{x})$ model that

has the following features. The top stage of the BCGP model can be viewed as the sum of a global (mean) process, say $Y_G(\mathbf{x})$, and a local (deviation) process, say $Y_L(\mathbf{x})$. The global mean, say $y_G(\mathbf{x})$ which is a draw from $Y_G(\mathbf{x})$, is meant to be a flexible description of large-scale $y(\mathbf{x})$ trends. The local deviation, say $y_L(\mathbf{x})$ which is a draw from $Y_L(\mathbf{x})$, captures small-scale $y(\mathbf{x})$ changes about $y_G(\mathbf{x})$. Subsequent stages put a prior on the global and local process parameters that ensure $y_G(\mathbf{x})$ draws are smoother than $y_L(\mathbf{x})$ draws. Another ingredient of the BCGP is that it contains a model parameter which allows the data to weight the effect of the global and local processes. Lastly, the BCGP can describe $Y(\mathbf{x})$ having heteroscedastic process variability by using a latent variable process to describe the variance of $Y(\mathbf{x})$. The method of prediction described in this paper allows one to estimate the global and local components of $y(\mathbf{x})$. The resulting predictions can be used, say, to determine the sensitivity of $y_G(\mathbf{x})$ to each input. Figure 8 of Example 4.3 illustrates this approach.

One area for future research is refinement of the prior, components of which have been selected for their analytic tractability. Most of our hyper-parameter choices have been made to reflect vague prior information; however, the choice of the hyper-parameters α_ω and β_ω for the ω prior are critical in determining the properties of the predicted $y_G(\mathbf{x})$ and $y_L(\mathbf{x})$. We have examined the global smoothness of the predicted $y_G(\mathbf{x})$, the centeredness of the predicted $y_L(\mathbf{x})$ about zero, and their relative smoothness for varying α_ω and β_ω . These properties were gauged heuristically in a test series of analytic examples having known $y_G(\mathbf{x})$ which was perturbed by a $y_L(\mathbf{x})$ having low-activity inputs. The final choice of parameters for the ω prior was made based on the ability to predict the $y_G(\mathbf{x})$. Analysts in different subject matter areas should do such an assessment using test beds drawn from their applications. This intuitive method of selecting a prior is not the only option for applying the prediction methodology introduced in this paper. Two alternatives are the use of Reference Priors as described in Gu *et al.* (2018) and the prior used for the widely-used Bayesian calibration software GMSPA that is introduced in Higdon *et al.* (2004, 2008) (see also Gattiker, 2008).

The methods and priors described in this paper are implemented in Matlab code that was used to run the examples in Section 4. This code is available from the first author.

ACKNOWLEDGMENTS

This material was based upon work partially supported by the National Science Foundation under Grants DMS-0806134 and DMS-1310294 to The Ohio State University and under Grant DMS-1638521 to the Statistical and Applied Mathematical Sciences Institute. Any opinions, findings, and conclusions or recommendations expressed in this material are those of the author(s) and do not necessarily reflect the views of the National Science Foundation.

References

- Ba, S. and Joseph, V. R. (2012). Composite Gaussian process models for emulating expensive functions. *Annals of Applied Statistics*, **6**(4), 1838–1860.
- Ba, S. and Joseph, V. R. (2018). *CGP: Composite Gaussian Process Models*. R package version 2.1-1.
- Banerjee, S., Carlin, B. P., and Gelfand, A. E. (2004). *Hierarchical Modeling and Analysis for Spatial Data*. Chapman and Hall, New York.
- Breiman, L., Friedman, J. H., Olshen, R. A., and Stone, C. J. (1984). *Classification and Regression Trees*. Chapman & Hall, New York.
- Chipman, H. A., George, E. I., and McCulloch, R. E. (1998). Bayesian cart model search. *Journal of the American Statistical Association*, **93**(443), 935–960.
- Cressie, N. A. (1993). *Statistics for Spatial Data*. J. Wiley, New York, First edition.
- Davis, C. B. (2015). *A Bayesian approach to prediction and variable selection using nonstationary Gaussian processes*. Ph.D. thesis, The Ohio State University.
- Forrester, A., Sobester, A., and Keane, A. (2008). *Engineering design via surrogate modelling: A practical guide*. Wiley, Chichester, UK.
- Gattiker, J. R. (2008). Gaussian Process models for simulation analysis (GPM/SA) command, function, and data structure reference. Technical Report LA-UR-08-08057, Los Alamos National Laboratory.

- Gelman, A., Roberts, G., and Gilks, W. (1996). Efficient Metropolis jumping rules. In J. M. Bernardo, J. O. Berger, A. P. Dawid, and A. F. M. Smith, editors, *Bayesian Statistics 5: Proceedings of the Fifth Valencia International Meeting*, pages 599–608. Oxford University Press, Oxford.
- Gramacy, R. B. and Lee, H. K. H. (2008). Bayesian treed Gaussian process models with an application to computer modeling. *Journal of the American Statistical Association*, **103**(483), 1119–1130.
- Gramacy, R. B. and Lee, H. K. H. (2012). Cases for the nugget in modeling computer experiments. *Statistics and Computing*, **22**(3), 713–722.
- Gu, M., Wang, X., and Berger, J. O. (2018). Robust gaussian stochastic process emulation. *Annals of Statistics*, **46**, 3038–306.
- Higdon, D., Kennedy, M., Cavendish, J., Cafoe, J., and Ryne, R. (2004). Combining field data and computer simulations for calibration and prediction. *SIAM Journal of Scientific Computing*, **26**, 448–466.
- Higdon, D., Gattiker, J., Williams, B., and Rightley, M. (2008). Computer model calibration using high dimensional output. *Journal of the American Statistical Association*, **103**, 570–583.
- Kennedy, M. and O’Hagan, A. (2001). Bayesian calibration of computer models (with discussion). *Journal of the Royal Statistical Society Series B*, **63**, 425–464.
- Lempert, R., Schlensinger, M. E., Bankes, S., and Andronova, N. (2000). The impacts of climate variability on near-term policy choices and the value of information. *Climate Change*, **45**, 129–161.
- Neal, R. (1998). Regression and classification using Gaussian process priors (with discussion). In J. M. Bernardo, J. O. Berger, A. P. Dawid, and A. F. M. Smith, editors, *Bayesian Statistics 6: Proceedings of the Sixth Valencia International Meeting*, pages 475–501. Oxford University Press, Oxford.
- Oakley, J. (2002). Eliciting Gaussian process priors for complex computer codes. *Journal of the Royal Statistical Society, Series D*, **51**(1), 81–97.

- Oakley, J. and O'Hagan, A. (2004). Probabilistic sensitivity analysis of complex models: A Bayesian approach. *Journal of the Royal Statistical Society Series B*, **66**, 751–769.
- O'Hagan, A. (1978). Curve fitting and optimal design for prediction (with discussion). *Journal of the Royal Statistical Society B*, **40**, 1–42.
- Ong, K., Santner, T., and Bartel, D. (2008). Robust design for acetabular cup stability accounting for patient and surgical variability. *Journal of Biomechanical Engineering*, **130**, 1–11.
- Qian, P. Z., Seepersad, C. C., Joseph, V. R., Allen, J. K., and Wu, C. F. J. (2006). Building surrogate models with details and approximate simulations. *ASME Journal of Mechanical Design*, **128**, 668–677.
- Roberts, G. O. and Rosenthal, J. S. (2001). Optimal scaling for various Metropolis–Hastings algorithms. *Statistical Science*, **16**(4), 351–367.
- Roberts, G. O., Gelman, A., and Gilks, W. R. (1997). Weak convergence and optimal scaling of random walk Metropolis algorithms. *The Annals of Applied Probability*, **7**(1), 110–120.
- Sacks, J., Welch, W., Mitchell, T., and Wynn, H. (1989). Design and analysis of computer experiments. *Statistical Science*, **4**(4), 409–435.
- Santner, T. J., Williams, B. J., and Notz, W. I. (2018). *The Design and Analysis of Computer Experiments, Second Edition*. Springer Verlag, New York.
- Villarreal-Marroquín, M. G., Chen, P.-H., Mulyana, R., Santner, T. J., Dean, A. M., and Castro, J. M. (2017). Multiobjective optimization of injection molding using a calibrated predictor based on physical and simulated data. *Polymer Engineering & Science*, **57**(3), 248–257.
- Xiong, Y., Chen, W., Apley, D. W., and Ding, X. (2007). A non-stationary covariance-based kriging method for metamodelling in engineering design. *International Journal for Numerical Methods in Engineering*, **71**, 733–756.